Proceedings of ASME Turbo Expo 2019:
Turbomachinery Technical Conference and Exposition
GT2019
June 17-21, 2019, Phoenix, Arizona, USA

GT2019-91428

A PNEUMATIC PROBE FOR MEASURING SPATIAL DERIVATIVES OF STAGNATION PRESSURE

C.J. Clark, S.D. Grimshaw
Whittle Laboratory
University of Cambridge
Cambridge, CB3 0DY, UK
Email: cjc95@cam.ac.uk

ABSTRACT

This paper introduces a pneumatic 9-hole probe which can measure flow angles, stagnation and static pressures, and spatial derivatives of stagnation pressure. It does this through direct measurement at a single location, rather than empirical corrections using measurements at multiple points.

The new design resembles a 5-hole probe with 4 additional holes positioned around the side of the probe head. This arrangement enables the probe to distinguish between flows with stagnation pressure gradient and flows at an angle. Mapping between the inputs, the probe hole pressures, and outputs, the calibration reference measurements, is achieved with a trained neural network which takes the place of a conventional calibration map.

Measurements of an unknown wake are performed in a calibration tunnel. The 9-hole probe data is compared with measured reference data and a "conventional" analysis of the 5 forward facing holes. The 5-hole probe analysis results in a maximum yaw angle error of 8.4°*, while the 9-hole probe matches the reference to within* 0.8°*. Mass-averaged stagnation pressure and kinetic energy loss coefficients, evaluated with the 5-hole probe analysis, result in errors of* $+2.8\%$ *and* -48% *respectively, while the 9-hole probe gives* $+0.5\%$ *and* -4.5%*.*

The new probe is used to perform an area traverse of an inlet guide vane in a research compressor. The 5-hole probe analysis gives a $\pm 5.5^\circ$ *variation in yaw angle across the wake and this reduces to* $\pm 1.0^\circ$ *when the 9-hole probe is used. Measurement of stagnation pressure gradient and curvature, based on single point measurements, is also demonstrated.*

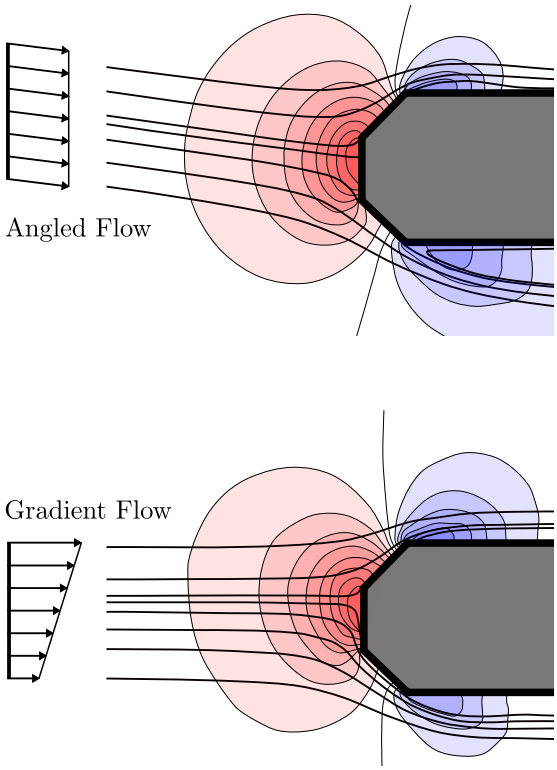

FIGURE 1: CFD simulated static pressure contours around a probe head in flows at an angle and with a stagnation pressure gradient. The same pressures are induced on the forward facing surfaces while pressure fields of opposite orientation occur on the sides.

INTRODUCTION

The aim of this work is to improve the accuracy of pneumatic probe measurements in flows with stagnation pressure spatial derivatives. Multi-hole pneumatic probes are widely used in research and industrial applications where robust, cheap (compared to optical measurements) flow surveys are required; a review of the 240 papers submitted to the Turbomachinery Committee of the ASME Turbo Expo in 2015 shows that 22% include steady measurements using multi-hole probes. Developments in multi-hole probe design and data reduction are briefly reviewed in the first part of this section.

Pneumatic probes measure incorrect pressures and flow angles when used in flow fields with stagnation pressure gradients. However, most flows of interest include stagnation pressure gradients caused by phenomena such as blade wakes and end wall boundary layers. The second part of this section reviews why these errors occur, looks at existing correction methods, comments on why corrections are not more widely used and highlights how the approach presented in this paper is different.

Multi-hole pneumatic probe development

The use of multi-hole pneumatic probes for time-averaged measurement of stagnation and static pressures and flow angles, is well established. Bryer and Pankhurst [1] describe the manufacture, calibration and use of 5-hole probes while Gallington [2] and Everett [3] introduce the 7-hole probe. Many papers have been published on pneumatic probes and most can be grouped into one or more of the following categories: data reduction techniques and extending angle range [4–9]; effect of probe Reynolds number [10–13], error analysis and improving experimental accuracy [14–16]; miniature probes and optimising settling time [17–19]. One thing common to all of these studies is that the pneumatic probe is calibrated in *uniform flow*.

Probe measurements in stagnation pressure gradients

In a flow with a stagnation pressure gradient (also considered as a velocity shear flow in some studies) a pneumatic probe deflects streamlines causing the probe to measure a stagnation pressure higher than that at the geometric centre of the probe. This effect was reported for Pitot tubes by Young and Maas in the 1930s [20] and since then researchers have addressed the issue by applying a "displacement correction" which is proportional to a non-dimensional spatial derivative of stagnation pressure (or velocity). The constant of proportionality has been determined experimentally [21–23] and analytically [24, 25].

Dixon [26] identifies the issue of measuring flow angle in shear flows. In his work flow angle errors are corrected by extrapolating measurements of geometrically-similar multi-hole probes of varying diameters to zero size, in order to evaluate the "true" flow angle. Ligrani *et al.* [27] apply an offset to their data to collapse the pressure measurements to one point in space. They then employ a correction to the transverse velocity components, based on velocity gradient, which is similar to Pitot tube corrections for axial velocity. Chernorary and Hjärne [28] uses the same approach as Ligrani to correct 5-hole probe measurements downstream of an outlet guide vane (OGV) cascade. Reference velocities are provided by a hotwire traverse and a linear relationship between non-dimensional velocity gradient and velocity error is measured across the OGV wake. This data is used to apply the displacement correction for an area traverse downstream of the OGVs and the corrected velocities are shown to agree well with reference measurements. Other researchers have applied similar methods for stagnation pressure [29] and velocities [30].

These displacement correction methods use pneumatic probes calibrated in uniform flows. The probes are unable to measure stagnation pressure gradients at a single spatial location and instead evaluate gradients from multiple measurement points and use a linear model relating gradient to velocity error to make corrections. This approach is limited in three ways. First, the constant of proportionality relating flow gradient to velocity error is a function of probe geometry and is obtained empirically in each study, sometimes with *a posteriori* knowledge of the flow field to be measured. Second, at incidence, as the probe becomes a lifting body, the streamline displacement is expected to change. This would make the correction "constant" a function of flow angle, unless the probe is nulled in both transverse directions. Third, the flow gradients used in the correction are calculated from multiple measurement points meaning the corrected velocities are dependent on resolution of the traverse grid.

It is noted that some studies consider stagnation pressure gradients and some velocity gradients. Velocity gradients, however, introduce an additional complication since variations can be due to stagnation or static pressure variations. In this paper stagnation pressure gradients are studied as these are associated with turbomachinery blade wakes.

Approach and layout of paper

The approach adopted is to develop a probe which can measure spatial derivatives of stagnation pressure *directly* using a calibration, and which does not require empirical displacement corrections. Through better knowledge of the flow conditions around the probe tip, the accuracy of measured flow properties are improved.

The paper is organised into five sections. In the first, the probe design and data reduction methods are explained and in the second, the calibration facility and procedure is described. The third section presents results from the calibration facility where 9-hole probe and 5-hole probe measurements are compared with reference data. In the fourth section, area traverse measurements downstream of inlet guide vanes in a research compressor are presented. Finally, there is a discussion of the implications of this work and suggestions for future study.

PROBE DESIGN

Conventional, multi-hole pneumatic probes are unable to determine the difference between an angled flow and a stagnation pressure gradient. Figure 1 shows a cross section of the flow pattern around a pneumatic probe head in these two flow conditions, simulated using CFD. Static pressure contours show that the probe surfaces where holes are conventionally placed for either 5- or 7-hole probes, i.e. the front face and angled facets, measure the same pressures whether in angled or gradient flow. Therefore, for conventional probes calibrated in a uniform stagnation pressure jet, both cases shown in Fig. 1 are measured as an angled flow.

This problem is also apparent when probe coefficients are considered. Attempts to measure the gradient using finite-differencing, between the holes, yield a "gradient coefficient", shown in Eq. 1, which is is equal to the traditional yaw coefficient. However, using finite differences to estimate the stagnation pressure curvature yields a new coefficient, Eq. 2. This curvature coefficient has previously been formed for use in error detection techniques [19].

$$C_{\nabla} = \frac{P_L - P_R}{dh_{probe}} = C_{\alpha} \tag{1}$$

$$C_{\nabla^2} = \frac{P_L - 2P_C + P_R}{dh_{probe}} \tag{2}$$

$$dh_{probe} = P_C - 0.25(P_L + P_R + P_U + P_D) \tag{3}$$

Conventional 5- and 7-hole probes are unable to distinguish between flow angles and gradients so additional information is required. Further inspection of Fig. 1 reveals differences between the flow fields behind the angled facets: The two flow conditions cause an asymmetric pressure field of opposite orientation on each side of the probe. The region of low static pressure caused by the gradient is limited to the first diameter downstream from the probe tip, while the disturbance caused by the yaw persists much further. This effect can be understood by considering the flow along an infinite cylinder. Parallel streamlines of a gradient flow, aligned with the axis of the cylinder, result in uniform static pressure around the circumference. However, angled flow induces a potential field as it passes around the cylinder. The new probe design introduced in this paper uses these differences to separate gradient flows from angled flows.

Figure 2 shows the new probe geometry. A single central tube of diameter $0.64mm$ is surrounded by 8 smaller tubes of diameter $0.41mm$ to achieve a tight packing and an overall probe head diameter of $1.5mm$. The probe head is ground such that two holes are located symmetrically on each 45° facet leaving a single hole on the front face. One hole on each 45° facet is sealed and ground flush. Holes are then drilled through the probe sidewalls into the sealed tubes, one diameter downstream of the probe tip. The resulting probe has a central hole and 4 forward facing holes on the 45° facets, the same as a conventional 5-hole probe setup. In addition it has 4 holes on the side of the probe to exploit the flow differences observed in Fig. 1. The labelling convention used is shown in Fig. 2, with centre, left, right, up, down representing the conventional holes and east, west, north, south the new side holes.

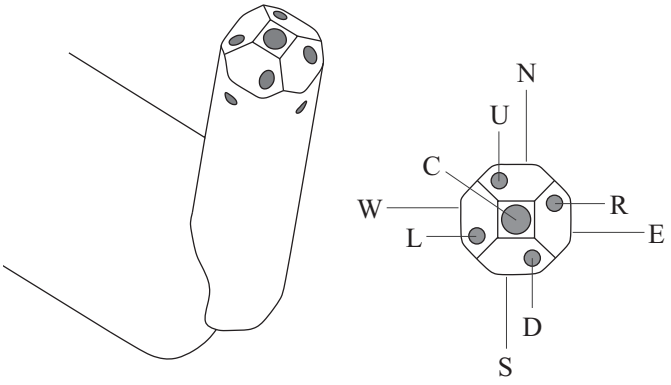

FIGURE 2: 9-hole probe and hole labelling convention.

Mapping between calibration data and test measurements is traditionally performed using pre-formed coefficients [10]. When measuring an unknown flow field these coefficients are evaluated from the probe head measurements and interpolated to give flow angles and pressures. A typical calibration results in a flow condition being defined by yaw angle, pitch angle and in some cases Reynolds number and/or Mach number. To this list, our new probe adds non-dimensional stagnation pressure gradients and curvatures in two directions. The stagnation pressure spatial derivatives are made non-dimensional so that at similar flow conditions, as viewed by the probe, the flow condition variables are represented as a single output value. The non-dimensional groups chosen are defined as:

$$\left(\frac{\partial P_0}{\partial x}\right)^* = \left(\frac{\partial P_0}{\partial x}\right)\left(\frac{D_{probe}}{P_0 - P_s}\right) \tag{4}$$

$$\left(\frac{\partial^2 P_0}{\partial x^2}\right)^* = \left(\frac{\partial^2 P_0}{\partial x^2}\right)\left(\frac{{D_{probe}}^2}{P_0 - P_s}\right) \tag{5}$$

The increase in the number of probe head measurements and flow condition variables means traditional interpolation, using pre-defined coefficients, is no longer practical.

The solution adopted is to use a neural network to map between measured pressures and flow condition variables. Neural networks are gaining popularity as a robust method to perform regression in many dimensions across curves of arbitrary

complexity. The use of neural networks has been demonstrated for conventional multi-hole probes by Rediniotis [14] and Conlon [31]. The neural network inputs are non-dimensionalised hole pressures, for example:

$$C_L = \frac{P_C - P_L}{dh_{probe}} \tag{6}$$

The outputs consist of flow angles, non-dimensional stagnation pressure derivatives in two directions, and stagnation and dynamic pressure coefficients. This results in 8 inputs and 8 outputs, however in this work, only the spatial derivatives in the yaw angle direction are calibrated, giving 6 outputs.

The neural network used is called a "multi-layer perceptron", comprising of a pass-through input layer, two hidden layers utilizing the ReLU activation function [32] shown in Eq. 7, and a final output layer.

$$ReLU(z) = max(0, z) \tag{7}$$

It is found that 80 neurons in each hidden layer gives a good compromise between over and under-fitting. This value is selected based on "leave-one-out" validation of the model, where 4 out of 5 calibration datasets are used for training and the final one is used for validation. This was cycled through all 5 combinations to evaluate the robustness of the model's hyper-parameters.

The model is trained using the LBFGS algorithm [33] to select weightings at each neuron as it is well suited to problems with a large number of parameters. To successfully train the network the most challenging step is to gather sufficient data describing combinations of flow angles and stagnation pressure derivatives.

CALIBRATION DESIGN

To calibrate the probe in flows with varying yaw and pitch angles, and with different stagnation pressure spatial derivatives, an existing Whittle Laboratory calibration facility was modified, Fig. 3. A centrifugal pump draws air through the inlet bellmouth, nozzle, and working section and a throttle is used to set the calibration jet speed.

Probes are mounted in the centre of the jet $20D_{probe}$ downstream of the nozzle exit. The probe stem is fixed to a motorised rotary table which sets the yaw angle of the probe to an accuracy of 0.1°. The pitch angle of the probe is set by positioning the gimbals on which the rotary table is mounted. The gimbals rotate about the position of the probe head and are also motorised; pitch angle can be set to within 0.1°.

Linear actuators with positional accuracy of $0.01mm$ are used to traverse cylindrical "wake bars" between the nozzle exit and the probe, and therefore introduce spatial derivatives of stagnation pressure to the calibration jet. These can be reorientated relative to the probe, so that stagnation pressure spatial derivatives in multiple directions can be generated. Other options for generating stagnation pressure derivatives were considered including variable porosity grids and fully developed pipe flow. Wake bars are chosen because they can be positioned accurately relative to the probe and they produce a family of gradients and curvatures from a single bar. They also resemble the types of wakes seen in turbomachinery flows. Wake size can be varied by changing the bar diameter and/or by varying how far upstream of the probe the bars are mounted. All pressure measurements were taken with a Scanivalve DSA3217 16-channel pressure scanner with a range of $\pm 2.5kPa$, further details are given in [34].

Reference stagnation pressure measurements are made with a $0.40mm$ Pitot tube ($0.27\ D_{probe}$), aerodynamically nulled in the freestream calibration jet. The Pitot tube probe is mounted in place of the 9-hole probe so that its head is positioned in the same location as the 9-hole probe head. For the reference measurement, an automated traverse routine, with 101 points hyperbolically bunched around the peak of the wake, moves the bar past the Pitot tube. Figure 4(a) shows plots of stagnation pressure coefficient, Y_p, against wake position relative to the Pitot tube, for $0.42D_{probe}$ and $0.98D_{probe}$ wake bars. Y_p is defined as:

$$Y_p = \frac{P_{0,ref} - P_0}{P_{0,ref} - P_{s,ref}} \tag{8}$$

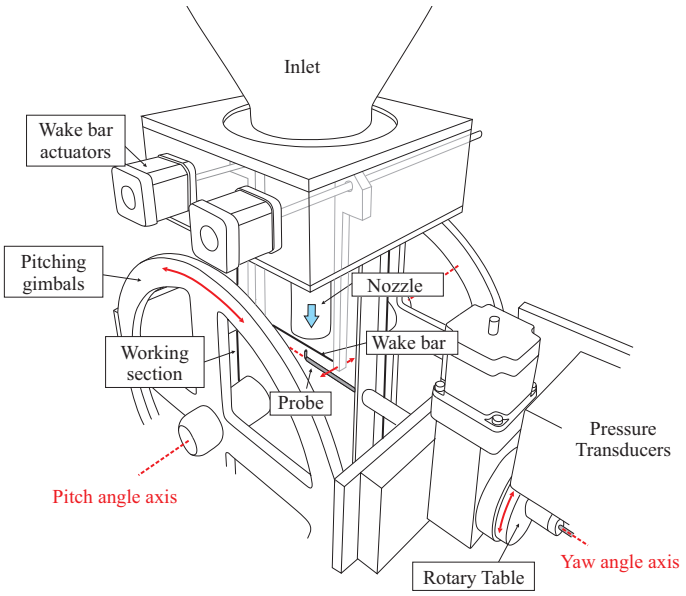

FIGURE 3: Schematic of calibration facility.

Calculating non-dimensional stagnation pressure gradients, and in particular curvature, from measurement data leads to significant scatter. These errors occur due to finite sampling. To smooth the spatial derivatives, Y_p profiles are fitted with a series of Gaussians with aligned centers. These analytic functions are then differentiated to give spatial derivatives. Figure 4(a) shows curves fitted to the Y_p data for two wake bars. For the 6 bar sizes tested the Gaussian curves fit well with the maximum difference in measured and fitted data less than 0.01 Y_p. Figure 4(a) also shows non-dimensional gradient and curvature plotted against position relative to the Pitot tube. Data from these plots is combined and gradient is plotted against curvature in Fig. 4(b). Zero curvature and gradient is at the centre of these plots, these are measurements taken either side of the wake in the freestream. As the Pitot tube passes through the wake a "ring-like" locus of points is generated relating gradient to curvature. Each wake bar has a different "ring" and by generating multiple rings a range of possible flow conditions can be mapped.

Figure 5 shows time-averaged yaw angle at three locations downstream of a circular cylinder at approximately $Re_{bar} = 4,000$ where Re_{bar} is based on upstream velocity and cylinder diameter. Yaw angles are calculated from time-averaged streamwise and lateral velocities reported by Ong and Wallace [35]. Accurate measurement of flow angle across the wake is not possible in the existing calibration facility, however, Fig. 5 shows that an assumption of constant flow angle is accurate to within $\pm 0.7^\circ$ at $10D_{bar}$, the location of the probe head downstream of the largest wake bar used for calibration. Also, constant flow angle implies that the static pressure is uniform across the wake because the streamlines are parallel. Static pressure is therefore measured with static tappings on the side wall of the working section, Fig. 3. In an improved set up, the flow angle and static pressure at the probe head location would be measured using a non-intrusive method, to provide a more accurate reference measurement for calibration.

The calibration facility movements (yaw, pitch and bar location) are automated and the flow angle ranges and step sizes are given in Table 1. The number of calibration points required is minimised by clustering the wake bar position based on the spatial derivatives. The reference Pitot measurement is used to generate the locations required to achieve points equispaced around the rings shown in Fig. 4(b). The spatial positions of these points are determined for each bar size and the corresponding coordinates are used to set the wake bar position for the 9-hole probe calibrations. For compatibility with the research compressor, the probe has an offset between the probe tip and its axis of rotation. The wake bar position during the traverse is therefore adjusted with an $L_{probe} \times cos(\alpha)$ offset so that the tip of the probe head is fixed relative to wake bar position as the probe is yawed.

Table 1 lists the calibrations and test cases performed in the calibration facility. The jet speed is set to give $Re_{probe} = 4,000$ for all calibrations and test cases as this approximately matches

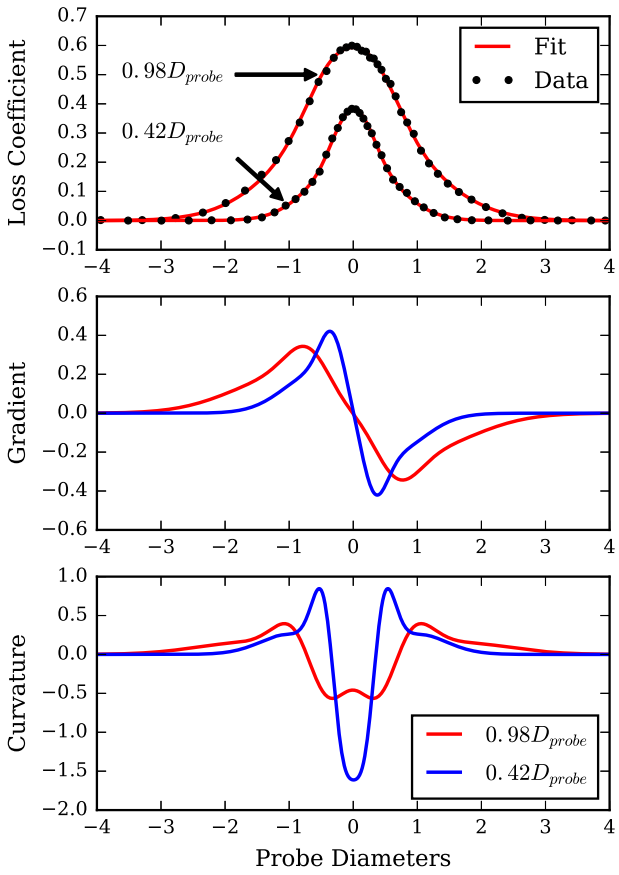

(a) Loss coefficient (Y_p), Gradient $\left(\frac{\partial P_0}{\partial x}\right)^*$ and Curvature $\left(\frac{\partial^2 P_0}{\partial x^2}\right)^*$

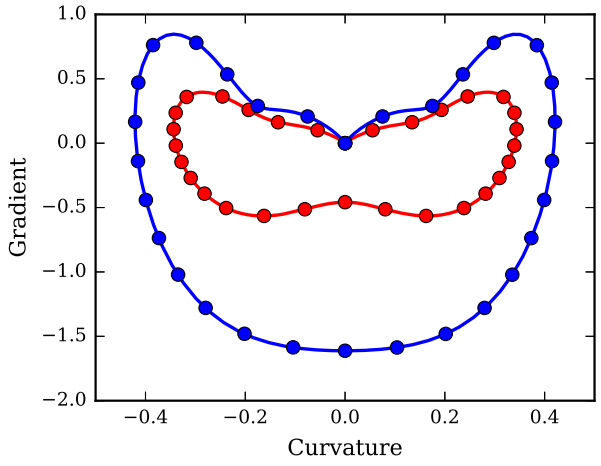

(b) Gradient $\left(\frac{\partial P_0}{\partial x}\right)^*$ against curvature $\left(\frac{\partial^2 P_0}{\partial x^2}\right)^*$ (lines) and clustered points used for calibration (circles)

FIGURE 4: Reference wake measurements.

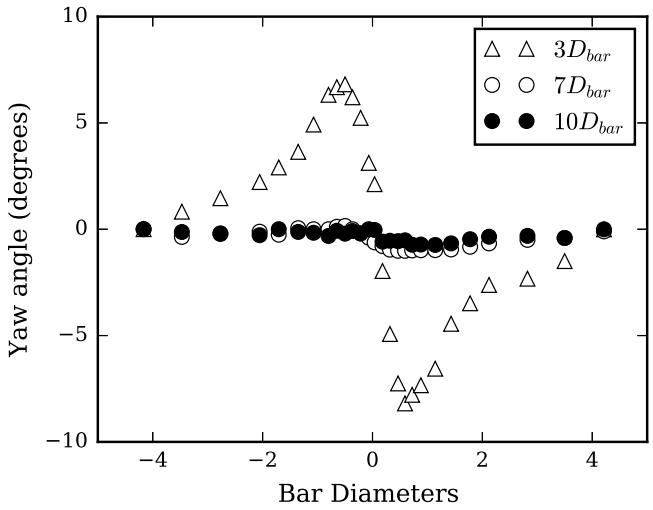

FIGURE 5: Flow angles downstream of a cylinder [35].

Re_{probe} in the turbomachinery measurement presented in this paper. Re_{probe} is based on upstream velocity and probe head diameter. For the calibrations reported in this paper, 6 bar sizes from $0.27D_{probe}$ to $1.08D_{probe}$ are used and the bars are traversed $10D_{probe}$ upstream of the probe head. This calibration ensures the probes operating range covers the flow angles and stagnation pressure spatial derivatives expected in a low speed turbomachinery test facility. The two-dimensional calibrations and test cases, i.e pitch angle $\beta = 0°$, are used in the next section and the three-dimensional calibrations are used to analyse the turbomachinery traverse data.

In the following sections the 9-hole probe measurements and data reduction are compared to a conventional 5-hole probe analysis using the same probe. For the 5-hole probe, calibrations without a wake bar are used to train a second neural network using the forward facing hole pressure coefficients (C_L, C_R, C_U, C_D) as inputs, and flow angles (α, β), stagnation pressure coefficient (C_{tot}) and dynamic pressure coefficient (C_{dyn}) as the flow condition variables. This approach removes any differences due to probe geometry or test run as the same test data is used to produce 9-hole and 5-hole probe results.

CALIBRATION RESULTS

Probe accuracy is assessed by measuring the flow field downstream of the $0.83D_{probe}$ wake bar. Two test cases were performed at flow angles of 0° and 10° with 81 points recorded across the wake traverse of each. The 9-hole probe neural network is trained using data from two larger and two smaller wake bars, Table 1, so that the $0.83D_{probe}$ wake bar is a "blind test", as it would be when using the probe in practice. Because the test case is performed in the calibration facility the reference measurements are used to assess the accuracy of both the 9-hole probe and 5-hole probe analyses.

TABLE 1: List of calibrations and test cases.

$\frac{D_{bar}}{D_{probe}}$	# x	α range	# αs	β range	# βs	# Total
Calibrations						
0.42	31	±20°	21	0°	1	651
0.72	31	±20°	21	0°	1	651
0.98	31	±20°	21	0°	1	651
1.08	31	±20°	21	0°	1	651
0.26	31	±20°	21	±5°	5	3255
0.42	31	±20°	21	±5°	5	3255
0.72	31	±20°	21	±5°	5	3255
Test Cases						
0.83	81	0°	1	0°	1	81
0.83	81	10°	1	0°	1	81

Figure 6 shows 5-hole and 9-hole probe yaw angle measurements compared with the reference. The 5-hole probe analysis shows a yaw angle swing, from 6.8° to −6.5°, as the probe passes through the stagnation pressure gradient of the wake. This error in yaw is because forward facing probe holes are unable to distinguish between gradient and flow angle as shown in Fig. 1. The 9-hole probe, however, is calibrated in stagnation pressure gradients and matches the reference flow angle to within ±0.6°. For the second test case, where the probe is at 10° incidence, Fig. 6(b) shows that the 5-hole probe analysis results in a maximum yaw angle error of 8.4° while the 9-hole probe is accurate to within 0.8°.

Figure 7 shows probe stagnation pressure measurements compared with the Pitot tube reference. At 0° yaw angle the 9-hole probe agrees with the reference to within ±0.01 while the 5-hole probe gives a loss coefficient 0.04 greater than the reference at the peak of the wake. This reduction in stagnation pressure at the centre of the wake is not, however, representative of a displacement error. It is hypothesised that the effect observed is due to a difference in yaw angle response between the Pitot and multi-hole probe, coupled with the unsteady flow angles within the wake.

At 10° incidence, the 5-hole probe analysis results in the wake being shifted $0.25D_{probe}$, compared to the reference. This spatial error is due to an "induced displacement" caused by overturning of the low momentum wake by the asymmetric, upstream

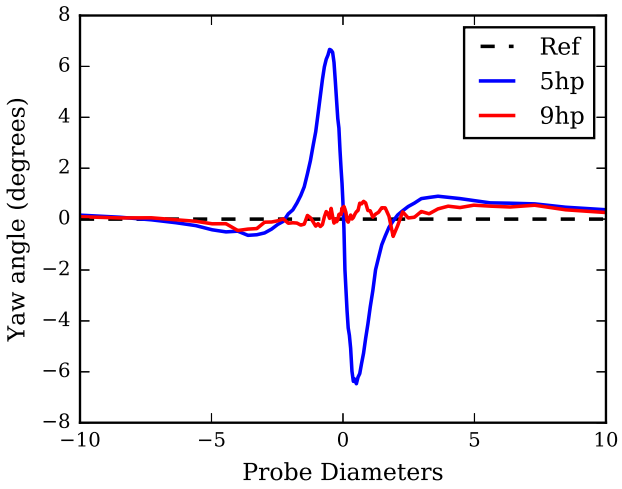

(a) Traverse at 0° incidence

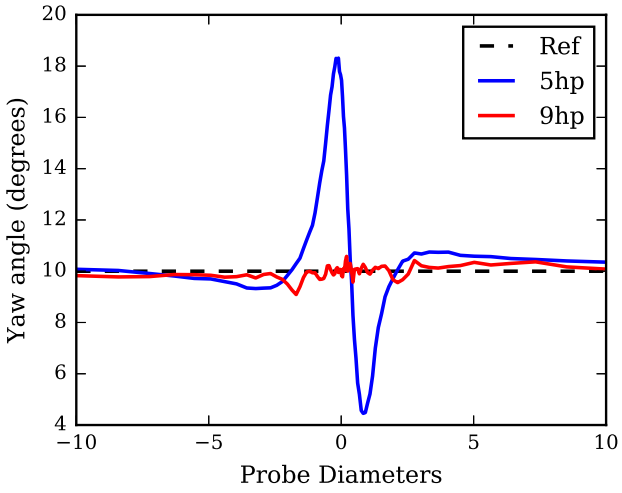

(b) Traverse at 10° incidence

FIGURE 6: Yaw angle (°)

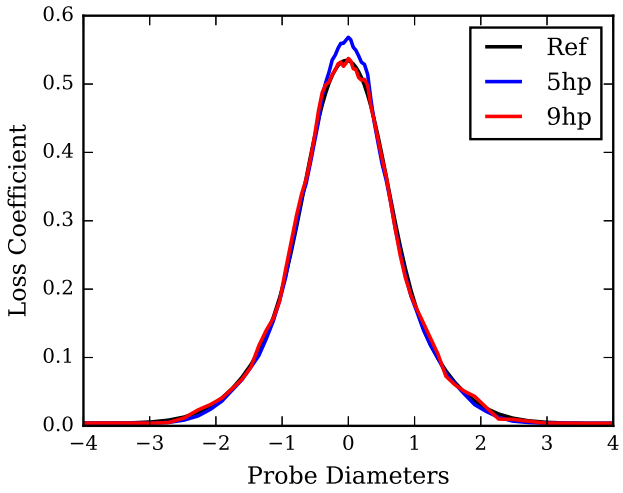

(a) Traverse at 0° incidence

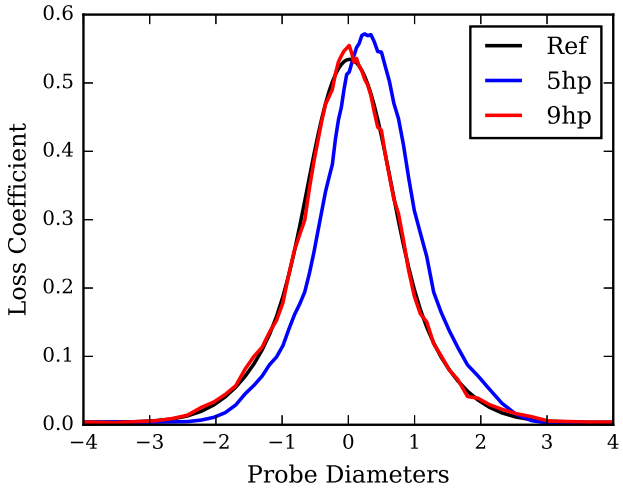

(b) Traverse at 10° incidence

FIGURE 7: Stagnation pressure loss coefficient, $Y_p = \frac{P_{0,ref} - P_0}{P_{0,ref} - P_{s,ref}}$

potential field of the probe at incidence. The 9-hole probe, however, identifies the flow condition correctly, implicitly accounts for the "induced displacement", and measures the wake in its correct position.

Figure 8 shows that the 5-hole probe measures reduced static pressure throughout the wake, with the largest discrepancies coinciding with the positive curvature regions at the edges of the wake. The effect this has on flow velocity is shown in Fig. 9 where the velocity ratio is increased across the entire wake compared to the reference measurement. Integrating the 5-hole probe mass flux between $\pm 10 D_{probe}$ to represent a turbomachinery blade pitch results in an additional 1.2% mass flow compared to the reference. Integrating the 9-hole probe measurement reduces the mass flow error to 0.1%.

To evaluate the overall effect of probe measurement errors, two loss coefficients are used, Eqs. 9 and 10, mass-averaged over $\pm 10 D_{probe}$. The results are given in Table 2 and show that the increased flow rate given by the 5-hole probe measurements increases $\overline{Y_p}$ at 0° incidence by 2.8% and reduces $\overline{Y_{KE}}$ by 48%. The kinetic energy loss coefficient error is particularly large for the 5-hole probe analysis due to its dependence on velocity ratio. This result shows that loss criteria dependent on static pressure measurements, such as kinetic energy loss coefficients, should be avoided when using conventional multi-hole probes. The 9-hole probe provides a better agreement for both $\overline{Y_p}$ and $\overline{Y_{KE}}$, giving

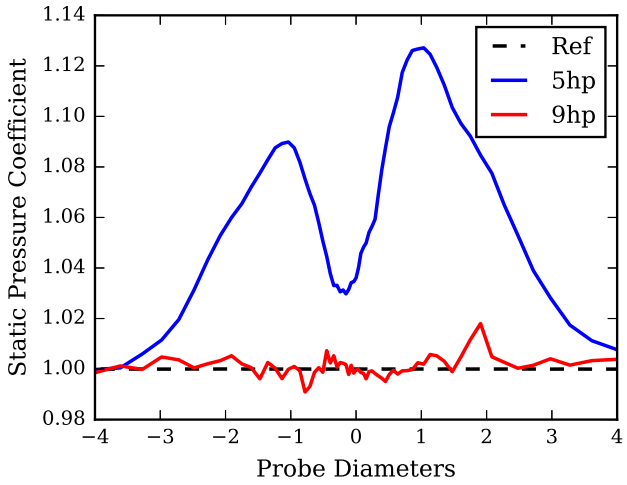

FIGURE 8: Static pressure coefficient, $C_p = \frac{P_{0,ref} - P_s}{P_{0,ref} - P_{s,ref}}$, traverse at 0° incidence.

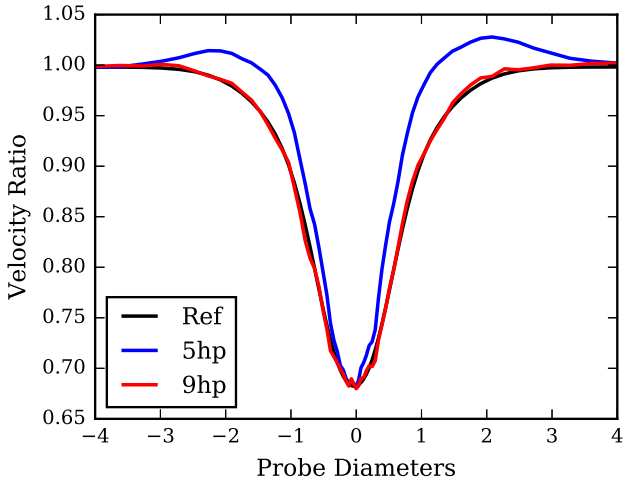

FIGURE 9: Velocity Ratio, $VR = \frac{V}{V_{fs}}$, traverse at 0° incidence.

results within 0.5% and 4.5% of the reference data, respectively.

$$Y_p = \frac{P_{0,ref} - P_0}{P_{0,ref} - P_{s,ref}} \tag{9}$$

$$Y_{KE} = 1 - \frac{\rho V^2}{\rho {V_{ref}}^2} \tag{10}$$

Table 2 shows similar trends at 10° incidence, with the error

TABLE 2: Mass-averaged $\overline{Y_p}$ and $\overline{Y_{KE}}$ from different probes at 0° and 10° incidence.

Probe	$\overline{Y_p}$,0°	$\overline{Y_{KE}}$,0°	$\overline{Y_p}$,10°	$\overline{Y_{KE}}$,10°
Ref	4.36%	4.36%	4.36%	4.36%
$9-hole$	4.38%	4.17%	4.38%	4.20%
$5-hole$	4.48%	2.25%	4.44%	2.62%

in spatial location of the wake, seen in the 5-hole probe measurements, having little effect on measured average loss values.

Figure 10 shows reference and measured spatial derivatives across the wake. The reference data is calculated from the Gaussian curve fitted to the reference Pitot tube data. Non-dimensional gradient and curvature measured with the 9-hole probe agree well with the reference data with peak errors of 0.02 and 0.12 respectively. The larger scatter in the curvature measurements occur due to its higher rate of change across the wake. Small ($< 0.05mm$) spatial misalignments between the reference Pitot and 9-hole probe during calibration are amplified by this high rate of change. This causes moderate errors in the curvature training data and the discrepancies seen in Fig. 10(b) are due to the network interpolating between these errors.

A 5- or 7-hole probe fabricated from $0.41mm$ hypodermic tube could have a probe head diameter 90% of the 9-hole probe. Flow angle errors due to stagnation pressure gradients are proportional to probe head diameter so a smaller probe head will result in proportionally lower errors. However, results in this section show that a conventional pneumatic probe head would need to be reduced in size by almost an order of magnitude to match the accuracy of the 9-hole probe when measuring wakes comparable in size to those tested here.

TURBOMACHINERY MEASUREMENTS

In order to use the probe for a blade passage measurement, the calibration is extended to include pitch angle. The flow field under investigation is 0.5 axial chords downstream of an inlet guide vane (IGV) row in a research compressor. Previous measurements show that at this location pitch angle varies by less than ±5° so calibrations from −5° to +5° were performed in 2.5° steps, Table 1. For these calibrations the wake bars are traversed in the yaw direction so stagnation pressure variations in the theta-direction can be detected (i.e. blade wakes) but variations in the radial direction can not (i.e. end wall boundary layers). The probe is designed to fit the compressor traverse gear and casing slot and the automatic traverse programme used is unmodified except to log the additional probe hole pressures measured with the 9-hole probe. The traverse consists of 21 radial points clustered towards the endwall and 61 circumferential points hy-

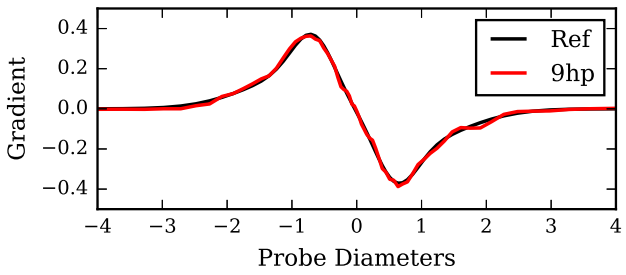

(a) Gradient, $\left(\frac{\partial P_0}{\partial x}\right)^*$

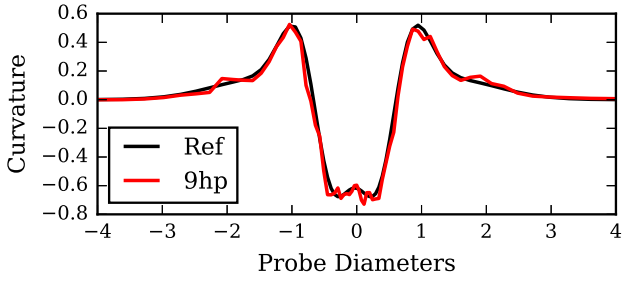

(b) Curvature, $\left(\frac{\partial^2 P_0}{\partial x^2}\right)^*$

FIGURE 10: Non-dimensional stagnation pressure gradient and curvature.

perbolically clustered on the IGV wake. The probe traverse is performed at a fixed yaw angle of 15°. Further details of the rig and traverse mechanism are given in [36].

Figure 11 shows contour plots of yaw angle downstream of the IGV row. Probe pressure measurements are analysed as a 5-hole and 9-hole probe in the same way as the test cases in the calibration facility. Contours of yaw angle are also plotted from a steady, Reynolds-Averaged Navier Stokes CFD simulation. Details of the solver and mesh are provided in [37] where similar computations are used to model the same compressor rig. CFD results are extracted at the same location as the measurement plane in the experiment.

At midspan the conventional 5-hole probe analysis shows a swing in yaw angle from 11.0° to 22.0° either side of the wake while the 9-hole probe show that this is reduced to a variation between 17.0° and 18.5°. The CFD shows a variation of ±0.4° across the wake at midspan. The comparison with CFD, combined with similar results from the calibration facility test cases, indicate that the variation in yaw angle measured by the 5-hole probe is an error. No significant errors arise at the endwalls suggesting that two-dimensional wakes, frequently seen in many aerospace applications, may only require the probe to be calibrated for stagnation pressure derivatives in a single direction. This significantly reduces the amount of calibration data required

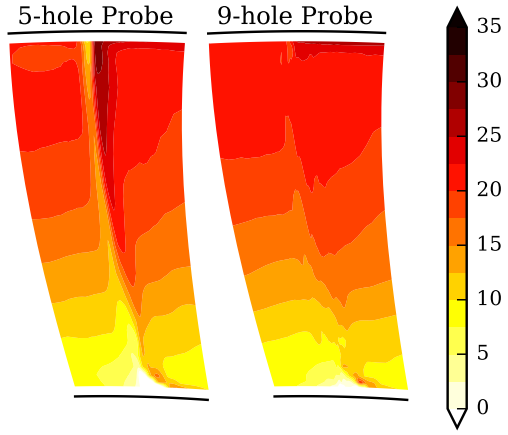

(a) Measured using 5-hole probe (left), 9-hole probe (right)

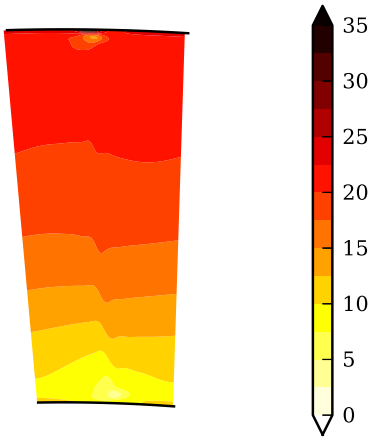

(b) Simulated with CFD.

FIGURE 11: Yaw angle (α) contours downstream of IGV

compared to a full calibration with derivatives in two directions.

Finally, a new type of measurement is presented in Fig. 12. This shows contours of non-dimensional pitchwise stagnation pressure gradient and curvature evaluated from single point measurements using the 9-hole probe. The spatial derivatives provide additional data on flow property variations between measurement locations and this can be used to reduce the required traverse resolution.

FUTURE WORK

This study shows that a probe able to detect spatial derivatives of stagnation pressure, can be manufactured, calibrated and used to test turbomachinery flow fields more accurately. It is suggested that future work, building on this proof of concept, could follow three routes:

First, improvements in the accuracy of the current imple-

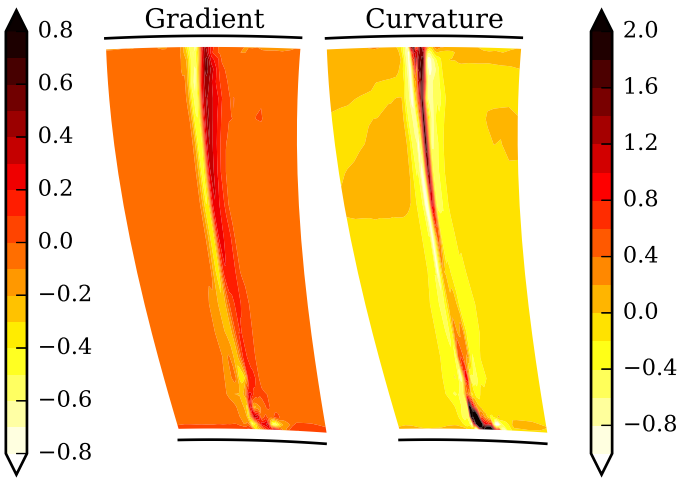

FIGURE 12: 9-hole probe measurements of pitchwise non-dimensional stagnation pressure gradient and curvature.

mentation are possible. The primary factor limiting accuracy is the reference measurement. With an ideal calibration the precision of the probe will tend to the precision of the reference. A number of limitations have been identified during the course of this work: The miniature Pitot tube used in the current study experiences small spatial derivative-based errors; the relative spatial location of the two probe tips can not be guaranteed and this causes errors in the curvature measurement; assumptions of constant static pressure and yaw angle could be updated by measuring the small variations ($< 0.7°$) greater than $10D_{bar}$ downstream of the wake bar. A carefully designed and implemented optical reference measurement could be used to address each of these issues.

The second route extends the flow conditions which can be identified by the probe. The effects of static pressure gradients, wall effects, or flow angle gradients could be addressed using a similar approach to that adopted here.

Finally, further development is required to enable adoption of this type of probe across the wider aerospace community. As more flow condition variables are included, e.g Mach and Reynolds number, the number of calibration points required increases. Therefore, work to increase the speed of the calibration process, through automated data gathering and/or the use of sparse calibration [38] is required. Alternatively, if manufacturing processes advance sufficiently and robust probe geometries are developed, multiple probes may share a single set of calibration data [39]. In this scenario increasingly complex calibrations become viable and calibration times becomes less important.

CONCLUSIONS

A new probe geometry has been designed and manufactured. The geometry resembles a conventional 5-hole probe, with the addition of 4 extra holes located a probe diameter behind the tip, facing orthogonal to the probe head axis. These additional holes enable the identification of stagnation pressure spatial derivatives.

Calibration of the probe has been undertaken in a modified facility. Variation of stagnation pressure gradient and curvature is achieved by passing wakes, caused by cylindrical bars of differing sizes, past the probe. Careful thought has been given to the clustering of measurements to minimize the calibration time required. The data is then used to train a neural network which maps probe hole pressures to flow condition variables.

The new probe and calibration technique is evaluated by measuring a previously unseen wake in the calibration facility. Comparison between a 5-hole probe analysis and the 9-hole probe highlights errors inherent in conventional probe measurements. Discrepancies in yaw angle, across the wake, were reduced from a maximum of $8.4°$ to $0.8°$. Large errors in static pressure, seen in the 5-hole probe measurements, were eliminated using the new probe. This results in the removal of a 1.2% mass flow error. It also reduces the mass-averaged stagnation pressure loss coefficient error, compared to a reference measurements, from 2.8% to 0.5%.

The probe calibration is extended to include pitch angle and the probe used to traverse the flow behind an inlet guide vane in a research compressor. The probe successfully identifies both the pitch-wise stagnation pressure gradients and curvatures, and measures yaw angles which agree with a RANS CFD simulation.

NOMENCLATURE

Symbols

α Yaw angle
β Pitch angle
x Spatial distance
ρ Density
C Coefficient
dh_{probe} Probe dynamic head
D_{bar} Wake bar diameter
D_{probe} Probe head diameter
L_{probe} Probe head length, axis of rotation to tip
P Pressure
V Velocity
Y_{KE} Kinetic energy loss coefficient
Y_p Stagnation pressure loss coefficient
Re_{bar} Reynolds Number based on wake bar diameter
Re_{probe} Reynolds Number based on probe head diameter

$\left(\frac{\partial P_0}{\partial x}\right)^*$ Non-dimensional stagnation pressure gradient

$\left(\frac{\partial^2 P_0}{\partial x^2}\right)^*$ Non-dimensional stagnation pressure curvature

$\overline{[\,]}$ Mass-averaged quantity

Subscripts

$[\,]_\Delta$ Gradient
$[\,]_{\Delta^2}$ Curvature
$[\,]_C$ Center
$[\,]_L$ Left
$[\,]_R$ Right
$[\,]_U$ Up
$[\,]_D$ Down
$[\,]_W$ West
$[\,]_E$ East
$[\,]_N$ North
$[\,]_S$ South
$[\,]_s$ Static
$[\,]_0$ Stagnation
$[\,]_{ref}$ Reference measurement
$[\,]_{fs}$ Freestream

Abbreviations

ReLU Rectilinear function
LBFGS Limited-memory Broyden-Fletcher-Goldfarb-Shanno Algorithm
RANS Reynolds-Averaged Navier Stokes
CFD Computational Fluid Dynamics

ACKNOWLEDGMENT

The authors would like to acknowledge Dr J. Taylor and Dr T. Hynes of the Whittle Laboratory for their thought provoking input during the course of this work. Thanks also to Dr W. Playford of Cambridge Aero-thermal Ltd for his assistance with probe manufacture. Further thanks go to Mr J. Eriksen and Mr F. Baseley of CUED for their work on the topic during summer placements, and finally to Prof. R. Miller for funding their time.

REFERENCES

[1] Bryer, D. W., and Pankhurst, R. C., 1971. *Pressure-probe methods for determining wind speed and flow direction*. HMSO.

[2] Gallington, R., 1980. "Measurement of very large flow angles with non-nulling seven-hole probes". *041 Force Academy*, p. 60.

[3] Everett, K., Gerner, A., and Durston, D., 1983. "Seven-hole cone probes for high angle flow measurement theory and calibration". *AIAA Journal,* ***21***(7), pp. 992–998.

[4] Ostowari, C., and Wentz, W., 1983. "Modified calibration technique of a five-hole probe for high flow angles". *Experiments in Fluids,* ***1***(3), pp. 166–166.

[5] Zilliac, G., 1993. "Modelling, calibration, and error analysis of seven-hole pressure probes". *Experiments in Fluids,* ***14***(1-2), pp. 104–120.

[6] Pisasale, A., and Ahmed, N., 2002. "A novel method for extending the calibration range of five-hole probe for highly three-dimensional flows". *Flow Measurement and Instrumentation,* ***13***(1-2), pp. 23–30.

[7] Yasa, T., and Paniagua, G., 2011. "Robust post-processing procedure for multi-hole directional probes". In Proceedings of ASME Turbo Expo.

[8] Benay, R., 2013. "A global method of data reduction applied to seven-hole probes". *Experiments in fluids,* ***54***(6), p. 1535.

[9] Shaw-Ward, S., Titchmarsh, A., and Birch, D. M., 2014. "Calibration and use of n-hole velocity probes". *AIAA Journal,* ***53***(2), pp. 336–346.

[10] Dominy, R., and Hodson, H., 1993. "An investigation of factors influencing the calibration of five-hole probes for three-dimensional flow measurements". *Journal of turbomachinery,* ***115***(3), pp. 513–519.

[11] Wenger, C. W., and Devenport, W. J., 1999. "Seven-hole pressure probe calibration method utilizing look-up error tables". *AIAA journal,* ***37***(6), pp. 675–679.

[12] Johansen, E. S., Rediniotis, O. K., and Jones, G., 2001. "The compressible calibration of miniature multi-hole probes". *Journal of Fluids Engineering,* ***123***(1), pp. 128–138.

[13] Crawford, J., and Birk, A. M., 2013. "Influence of tip shape on reynolds number sensitivity for a seven hole pressure probe". *Journal of Engineering for Gas Turbines and Power,* ***135***(9), p. 091602.

[14] Rediniotis, O. K., and Vijayagopal, R., 1999. "Miniature multihole pressure probes and their neural-network-based calibration". *AIAA journal,* ***37***(6), pp. 666–674.

[15] Reichert, B. A., and Wendt, B. J., 1994. "A new algorithm for five-hole probe calibration, data reduction, and uncertainty analysis".

[16] Sumner, D., 2002. "A comparison of data-reduction methods for a seven-hole probe". *Journal of Fluids Engineering,* ***124***(2), pp. 523–527.

[17] Naughton, J., Cattafesta III, L., and Settles, G., 1993. "Miniature, fast-response five-hole conical probe for supersonic flowfield measurements". *AIAA journal,* ***31***(3), pp. 453–458.

[18] Georgiou, D. P., and Milidonis, K. F., 2014. "Fabrication and calibration of a sub-miniature 5-hole probe with embedded pressure sensors for use in extremely confined and complex flow areas in turbomachinery research facilities". *Flow Measurement and Instrumentation,* ***39***, pp. 54–63.

[19] Grimshaw, S., and Taylor, J., 2016. "Fast settling millimetre-scale five-hole probes". In ASME Turbo Expo 2016: Turbomachinery Technical Conference and Exposition, American Society of Mechanical Engineers, pp. V006T05A014–V006T05A014.

[20] Young, A., and Maas, J., 1937. "The behavior of a pitot tube in a transverse total-pressure gradient. r & m 1770, 1936". *British ARC, and ARC,* ***2589***.

[21] MacMillan, F., 1956. "Experiments on pitot-tubes in shear flow".

[22] Chue, S., 1975. "Pressure probes for fluid measurement". *Progress in aerospace sciences,* ***16***(2), pp. 147–223.

[23] McKeon, B., Li, J., Jiang, W., Morrison, J., and Smits, A., 2003. "Pitot probe corrections in fully developed turbulent pipe flow". *Measurement Science and Technology,* ***14***(8), p. 1449.

[24] Hall, I., 1956. "The displacement effect of a sphere in a two-dimensional shear flow". *Journal of Fluid Mechanics,* ***1***(2), pp. 142–162.

[25] Lighthill, M., 1957. "Contributions to the theory of the pitot-tube displacement effect". *Journal of Fluid Mechanics,* ***2***(5), pp. 493–512.

[26] Dixon, S., 1978. "Measurement of flow direction in a shear flow". *Journal of Physics E: Scientific Instruments,* ***11***(1), p. 31.

[27] Ligrani, P., Singer, B., and Baun, L., 1989. "Spatial resolution and downwash velocity corrections for multiple-hole pressure probes in complex flows". *Experiments in Fluids,* ***7***(6), pp. 424–426.

[28] Chernoray, V., and Hjarne, J., 2008. "Improving the accuracy of multihole probe measurements in velocity gradients". In ASME Turbo Expo 2008: Power for Land, Sea, and Air, American Society of Mechanical Engineers, pp. 125–134.

[29] Town, J., Akturk, A., and Camc, C., 2013. "Gt 2012-69280 total pressure correction of a subminiature five-hole probe in areas of pressure gradients".

[30] Hoenen, H. T., Kunte, R., Waniczek, P., and Jeschke, P., 2012. "Measuring failures and correction methods for pneumatic multi-hole probes". In ASME Turbo Expo 2012: Turbine Technical Conference and Exposition, American Society of Mechanical Engineers, pp. 721–729.

[31] Conlon, M. J., Wright, A., and El Ella, H. M. A., 2017. "Measurement of large flow angles with non-nulling multi-hole pressure probes". In ASME Turbo Expo 2017: Turbomachinery Technical Conference and Exposition, American Society of Mechanical Engineers.

[32] Mitchell, T., 1997. *Machine Learning*. McGraw-Hill.

[33] Nocedal, J., 1980. "Updating quasi-newton matrices with limited storage". *Mathematics of computation,* ***35***(151), pp. 773–782.

[34] Scanivalve. "Scanivalve, DSA 3217/3218, Digital Sensor Array, Data Sheet No. G511".

[35] Ong, L., and Wallace, J., 1996. "The velocity field of the turbulent very near wake of a circular cylinder". *Experiments in fluids,* ***20***(6), pp. 441–453.

[36] Grimshaw, S., Pullan, G., and Walker, T., 2015. "Bleed-induced distortion in axial compressors". *Journal of Turbomachinery,* ***137***(10), p. 101009.

[37] Grimshaw, S., Pullan, G., and Hynes, T., 2016. "Modeling nonuniform bleed in axial compressors". *Journal of Turbomachinery,* ***138***(9), p. 091010.

[38] Shaw-Ward, S., McParlin, S. C., Nathan, P., and Birch, D. M., 2018. "Optimal calibration of directional velocity probes". *AIAA Journal*, pp. 1–10.

[39] Hall, B. F., and Povey, T., 2017. "The oxford probe: an open access five-hole probe for aerodynamic measurements". *Measurement Science and Technology,* ***28***(3), p. 035004.